Carbon 122 (2017) 411–421

Contents lists available at ScienceDirect

Carbon

journal homepage: www.elsevier.com/locate/carbon

The role of ozone in the formation and structural evolution of graphene oxide obtained from nanographite

Sam Groveman [a, b, c], Jing Peng [c, d], Boris Itin [e], Ibrahim Diallo [b, d], Lawrence M. Pratt [b], Alexander Greer [g, c], Elizabeth J. Biddinger [c, h], Steve G. Greenbaum [d, f], Charles Michael Drain [a, c], Lynn Francesconi [a, c], Michele Vittadello [b, c, *]

[a] Department of Chemistry, Hunter College of the City University of New York (CUNY), New York, NY 10065, USA
[b] Department of Chemistry and Environmental Science, Medgar Evers College of CUNY, Brooklyn, NY 11225, USA
[c] Ph.D. Program in Chemistry, The Graduate Center of CUNY, New York, NY 10016, USA
[d] Department of Physics, Hunter College of CUNY, New York, NY 10065, USA
[e] New York Structural Biology Center, New York, NY 10027, USA
[f] Ph.D. Program in Physics, The Graduate Center of CUNY, New York, NY 10016, USA
[g] Department of Chemistry, Brooklyn College of CUNY, Brooklyn, NY 11210, USA
[h] Department of Chemical Engineering, City College of New York, CUNY, New York, NY 10031, USA

ARTICLE INFO

Article history:
Received 27 February 2017
Received in revised form
21 June 2017
Accepted 22 June 2017
Available online 28 June 2017

ABSTRACT

Chemical exfoliation of graphite under strong oxidizing conditions yields graphene oxide nanosheets with oxy functional groups on the carbon basal plane. The importance of ozone in the chemical oxidation mechanism of graphite by the widely-used Hummers' method has been largely overlooked. Herein we demonstrate that the ozonolysis of graphite leads to the formation of secondary epoxy and peroxymonosulfate ester functional groups arising from a rotationally hindered Criegee intermediate and sulfuric acid, in a strongly favored thermodynamic process. This mechanistic step is followed by formation of adjacent epoxy and hydroxy groups as major functionalities on graphene oxides via a radical process, and leaves a significant amount of unreacted peroxides well above levels previously recognized. The thermal decomposition of graphene releases sulfur oxygen species (SO_2 and SO), but does not appear to release ozone even if this reaction pathway is moderately favored thermodynamically. We propose a new structural model for graphene oxide based on detailed chemical and spectroscopic data that provides insight into observed chemical reactivity and physical properties, including the antimicrobial activity and protein deactivation.

1. Introduction

The great potential of graphene oxide (GO) in fields such as electronics and optoelectronics is well recognized in connection with its solubility properties and the advantages associated with material processing in hydrophilic media [1]. GO is studied both as a precursor for graphene [2] and as a hole conductor in solar cells [3]. Other applications of GO extend into the field of biotechnology because its amphiphilic character allows stable adsorption of proteins and oligonucleotides to the surface [4,5]. However, progress in biotechnology research is stalled by the finding that GO is a very effective enzyme inhibitor [6]. The antibacterial properties of GO is linked to noncovalent adsorption on the carbon basal plane [7]. Also, residual oxidative debris (OD) in GO is linked to protein deactivation and toxic effects on human cell cultures [8]. The present work provides insights into the chemical reactivity of GO as another mechanism for enzyme inhibition and antibacterial activities.

GO suspensions are often prepared by variations of the Hummers' method which use permanganate and sulfuric acid [2,9]. The mechanism of GO formation is still poorly understood though the main steps are recognized [10,11]. It was proposed that graphite is first converted into a sulfuric acid/graphite intercalation material mediated by the generation of inorganic sulfates [10] in the exposed cavities, leaving room for the subsequent two-step

* Corresponding author. Department of Chemistry and Environmental Science, Medgar Evers College of CUNY, Brooklyn, NY 11225, USA.
E-mail address: mvittadello@mec.cuny.edu (M. Vittadello).

http://dx.doi.org/10.1016/j.carbon.2017.06.092
0008-6223/

oxidation of the carbon surface by manganese species [11]. Acidic water solubilization completes the exfoliation of graphite and partially removes the sulfate groups leading to GO monolayers and heavier aggregates [12,13]. However, the notion that sulfuric acid is solely responsible for the rapid exfoliation of graphite [10,14] is contrary to the expected reactivity of hydrophobic graphite with hydrophilic sulfuric acid. In this contribution we provide an alternative explanation addressing this conundrum that reconciles new and previously published data, including the observed reactivity of GO. There is evidence that GO can be prepared by ozonolysis of graphene using UV irradiation [15], and ozonation was proposed as a useful synthetic step for further functionalization [16]. The reactivity of graphite toward ozone was probed by vibrational spectroscopy, and the presence of metastable ozonides in graphitic oxide was previously hypothesized [17]. Up until very recently, ozone had not been clearly linked to the synthesis of GO from graphite using the Hummers' method, though permanganate and sulfuric acid are known to react to produce ozone [18,19]. Unlike with fullerenes [20], nanotubes [21], and polycyclic aromatic hydrocarbons [22], spectroscopy and DFT calculations on GO have provided no evidence for the presence of surface ozonides. It was previously reported that 1,3-dipolar cycloadditions and formation of primary ozonides from O_3 or S_3 take place with the smallest-diameter single-walled nanotubes (SWNTs) and not with flat graphite surfaces or large radius nanotubes in the dark [21]. Contrary to prior reports, Chen et al. have shown that the oxidation of graphite to GO can be explained by the presence of ozone under the conditions of the Hummer's method and selected modifications [19]. These authors demonstrated that the presence of additional water (unavoidable even with concentrated sulfuric acid) increases ozone production measured *in situ*, provided that the suspension is heated at 40 °C for 2 h after the initial low-temperature oxidation. A mechanism wherein ozone gives rise to atomic oxygen and hydroxyl radicals, which lead to the oxidation of graphite, was put forward. While it was implied that ozone can also react directly with graphite, it was not investigated how ozonolysis would occur as a possible oxidative pathway.

Various GO functional group stoichiometries are found depending on the synthetic approach and there is no consensus on a definitive structural model [23]. The Lerf-Klinowski [24] and the Szabo-Dékány [23] models seem to be the most consistent with the current body of data, even if they do not account for remaining sulfur species when sulfuric acid is used in the synthesis [13]. Both these models propose the existence of extended conjugated regions whose size depends on the C/O ratio (typically between 1.8 and 2.5). Functional groups on the surface include tertiary alcohols, epoxides, carboxylic acids, five- and six-membered ring lactols, and anhydrides [25]. Mono- and disubstituted sulfate esters, which are fairly stable to hydrolysis are also present [13] and can only be completely removed under strong basic treatment at the expense of disruption of other groups [26]. Keto-enol equilibria were suggested as the explanation for the pronounced acidity of GO (pH 2–3) as an alternative to the presence of carboxylic acids [12]. $2D^{13}C/^{13}C$ chemical-shift correlation solid-state NMR spectra unequivocally established that a large fraction of carbon linked to hydroxyl groups (C–OH) are also bonded to epoxide carbons [27]. The presence of OD add further complications to the structure and properties of GO [28,29].

Here we investigate the structure and composition of GO synthesized from nanographite, using a modified Hummers method with H_2SO_4 and $KMnO_4$. The temperature of the reaction was kept at 40 °C before raising it to 60 °C, in contrast to standard procedures (see Experimental section). After work-up, the sample was dried under high vacuum for five days (10^{-5} mbar). Our reaction conditions favor the formation of a GO with a high degree of oxidation (Supplementary Table 1). The tendency of the sample to explode above 175 °C complicates differential thermogravimetric analysis (Supplementary Fig. 1). We smelled the distinct odor of ozone during the synthesis and following an uncontrolled deflagration during heat-drying of a few grams of GO sample. These initial observations prompted an in-depth study of the resulting GO and its connection with ozone.

2. Experimental section

2.1. Graphene oxide (GO) synthesis

A 2-L beaker was filled with 460 mL of 95% H_2SO_4 and placed in an ice bath to cool to 0 °C. To the acid solution, 12 g of nanographite (Asbury Graphite Mills Inc.) was added. Over the course of 2 h, 60 g of $KMnO_4$ was added, keeping the solution temperature below 10 °C. The mixture was then heated to 39 °C for 2 h while stirring. The solution was then heated to 65 °C over the course of 30 min before being cooled back to 10 °C in an ice bath. Deionized (DI) water (920 mL) was slowly added to the solution, taking care to keep the temperature below 50 °C. The solution was stirred for 10 min and then split evenly between two 2 L beakers. To each beaker 1.25 L of DI water was added in small portions followed by 25 mL of 30% H_2O_2. The beakers were covered and left to settle overnight. The settled mixture was decanted and the supernatant discarded. The remaining mixture was divided into 50 mL centrifuge vials and centrifuged at 5000 rpm (with an Eppendorf 5424 bench-top centrifuge) for 15 min before being decanted again and discarding the supernatant. The precipitate in each vial was resuspended in 30 mL of 5% HCl before further centrifugation. The acid supernatant was decanted and discarded. This acid washing process was repeated six more times, after which the process was reiterated using DI water instead of acid. The graphene precipitate was dried via lyophilization for two days, and then on a high vacuum line (10^{-5} mbar) for five days. The residual water content was measured by means of a Karl-Fisher coulometric titration. C/H/O elemental analysis was conducted at Galbraith Laboratories.

2.2. KI treatment

Approximately 200 mg of GO was added to an empty 50-mL centrifuge vial. 0.5 M KI was added to a total volume of 30 mL in the vial. The vial was shaken vigorously for 1 h before being centrifuged at 5000 rpm for 15 min. The supernatant was decanted and discarded. The reaming precipitate was centrifuge washed five times with DI water as described above, before being dried via lyophilization and a high vacuum line.

2.3. $NaBH_4$ reduction

In a 1-L beaker, 830 mg of GO was suspended in 950 mL of DI water. The solution was sonicated in a Branson 1200 sonicator for 1 h at 35 °C. The solution was then heated to 60 °C while stirring and 900 mg of $NaBH_4$ was added slowly. The reaction was left to stir at 60 °C for 2 h. The reaction was then centrifuge-washed five times in DI water as described above, before being dried via lyophilization and a high vacuum line.

2.4. Differential thermogravimetry

GO (2–4 mg) was placed in a platinum pan and loaded into a Shimadzu DTG-60A thermal-gravimetric analyzer using α-alumina as reference. The sample was heated from 40 °C to 900 °C at a rate of 1 °C per-minute under air or argon.

2.5. Potentiometric ozone detection

GO samples with masses between 7.5 and 23.0 mg were placed in a septum-sealed 20-mL GC-MS headspace vial. The vial was heated (without explosion) for 5 min at 200 °C, after which 1 mL was transferred with a syringe to an ozone detection chamber through a silicon septum. The potentiometric ozone detection was carried out using a digitally-monitored ozone sensor (SainSmart MQ-131).

2.6. Gas analysis

Temperature programmed desorption (TPD) experiments were performed utilizing a Hiden HPR-20 R&D Atmospheric Pressure Gas Analysis System in multiplier mode for the mass spectrometer detector. To perform the analysis, 6.5–21.0 mg of GO sample was loaded between quartz wool plugs in a 4-mm diameter quartz tube. The sample tube was placed in a tube furnace. Argon was flowed at 30 mL/min through the sample tube and the product gas was analyzed using the gas analysis system (scanning from 1 to 100 amu) as a function of time. Once a stable baseline spectra was obtained, the sample was heated at 5 °C/min. A k-type thermocouple was used for both temperature control feedback and monitoring of the actual furnace temperature.

2.7. Singlet oxygen measurements

The singlet oxygen emission was assayed using a photomultiplier tube at an operating voltage of −650 V. One-gram quantities of GO were heated to 200 °C. The detection of $^1O_2$ luminescence used a NIR bandpass filter centered at 1270 nm (OD4 blocking, fwhm = 15 nm). The lack of a $^1O_2$ luminescence signal was based on an analysis on a 600 MHz oscilloscope.

2.8. High accuracy mass spectrometry measurements

GO sample. A Shimadzu GCMS-2020 gas chromatograph/single quadrupole, electron impact (−70 eV) mass spectrometer equipped with a Shimadzu DI-2010 direct insertion probe was used to analyze a GO sample (~0.7 mg). GO was introduced in a quartz capillary which was placed on the tip of the DI-2010 probe. After insertion into the GC-MS ion source, the probe was heated at 80 °C/min to 160 °C holding the temperature for 2 min, followed by a 5 °C/min ramp to 280 °C holding the temperature for 1 min. Scan was from 5.0 to 75.0 Da with a data acquisition rate of 0.10 s/scan, and the ion source temperature was set to 200 °C. As a reference standard for the mass calibration perfluoro *t*-butylamine (PFTBA) was analyzed in a separate run under similar MS settings (data not shown). Data were analyzed using the Cerno MassWorks software (Cerno Biosciences, ver. 4.0) equipped with calibrated line-shape isotope profile search (CLIPS).

Ozone standard. Ozone standards were prepared using an Enaly OZX-300 ST ozone generator set to generate ozone at ~200 mg/h. The ozone was introduced into the Shimadzu GCMS-2020 split/splitless injection port via a SGC 2.5-mL gas tight syringe equipped with a locking valve. The GCMS was run isothermally at 40 °C at 1 mL/min helium flow on a 5 m × 0.18 mm ID uncoated restrictor/guard column from Restek; the injection port, column, and interface were kept at 40 °C, and the ion source was kept at 200 °C. The scan range varied slightly from the GO sample (35–100 Da) as the nitrogen from the ozone standard would saturate the detector. For the first 3 min of the analysis, PFTBA was introduced as a reference standard for the Cerno software, then two 2.5 mL volumes of the ozone standard were manually injected.

2.9. TEM imaging

All data were collected at 200 kV on a Jeol 2100 transmission electron microscope equipped with EDAX at the eucentric point to ensure reproducibility of the measurements. A 10-μL drop of the GO dispersion was placed on a 300-mesh copper grid (TED Pella Inc.) and allowed to dry for several minutes before imaging.

2.10. XRD analysis

Samples were recorded with a Bruker D8 Focus X-ray diffractometer with $\lambda_{Cu,\alpha1}$ = 1.540600 Å and $\lambda_{Cu,\alpha2}$ = 1.544390 Å. The samples were measured in air within 1 h of leaving an Ar-filled glove box.

2.11. Colorimetric detection of peroxides

The presence of peroxides was detected by using a chromatic indicator (*N*,*N*-diethyl-p-phenyldiamine). The test was conducted along with controls on our GO, commercially available GO (Graphene Supermarket), and GO chemically reduced with $NaBH_4$ (R-GO).

15 mg of a powder mixture of chromatic indicator, potassium iodide, and sodium phosphate dibasic (Hach test kit model OZ-2) was measured out into several 1 mL centrifuge vials and dissolved in 500 μL of deionized water just before measurement.

A calibration curve was built by preparing, one at a time, four 1-mL solutions of 30% vol/vol H_2O_2 (Sigma-Aldrich) with concentration in the interval 0.392–3.916 mM 500 μL of each solution was added to an indicator vial and allowed to react for 2 min. The solution was then centrifuged at 15,000 rpm for 1.5 min on an Eppendorf 5434 centrifuge before being analyzed with a Shimadzu SolidSpec-3700 DUV spectrometer between 400 and 600 nm.

For the GO measurement, 11.8 mg of GO was suspended in 500 μL of deionized water and mixed for 1 h. This was combined with one of the indicator vials and allowed to react for 2 min, before centrifugation at 15,000 rpm for 1.5 min. The supernatant was then analyzed by a Shimadzu SolidSpec-3700 DUV spectrometer between 400 and 600 nm. The spectroscopic results were used in combination with the C/H/O elemental analysis results for quantitative estimations.

2.12. Trapping of peroxide with triphenylphosphine

The trapping studies were conducted in 600-μL suspension of 11.6 mg GO in CH_2Cl_2 and 45 mM PPh_3 stirred for 15 min at 25 °C. The yield of surface-bound peroxide (1.8% $g_O/g_{O_{Total}}$) was estimated on the basis of the reaction of PPh_3 to give O=PPh_3 and C/H/O elemental analysis results.

2.13. Infrared analysis

Medium IR spectra were recorded with a Thermo Scientific NICOLET 6700 spectrometer using a Specac MKII Golden Gate ATR cell. The cell was assembled inside an Argon dry-box. Each spectrum resulted from the average of 2000 scans with a resolution of 4 cm^{-1}. After background-correction the spectra were analyzed by Gaussian decomposition using the software IGOR Pro.

2.14. Nuclear magnetic resonance (NMR) measurements

^1H–^{13}C cross-polarization magic-angle spinning (CPMAS) NMR measurements were performed at a typical 15 kHz (±2 Hz) spinning speed and with a recycle delay of 2 s between successive acquisitions at 10,000 scans. Ramped-amplitude cross-polarization

[30], in which the proton field strength was varied linearly by 50%, was implemented to compensate for inhomogeneous radio-frequency fields across the sample. 5 ms ^{1}H spin-lock times were used to transfer magnetization from ^{1}H to ^{13}C nuclear spin baths, and high-power heteronuclear proton decoupling (80 kHz) was achieved using the TPPM composite pulse sequences [31]. Measurements were conducted on Bruker spectrometers (Bruker BioSpin Corp. Billerica, MA) operating at ^{1}H frequencies of 750 MHz (Avance I) and equipped with a 4 mm HFX probe. All spectral datasets were processed with 100 Hz of line broadening; chemical shifts were referenced externally to the methylene ($-CH_2-$) group of adamantane (Sigma) at 38.48 ppm [32].

^{13}C NMR experiments were carried out on a Varian solid state NMR spectrometer operating near 125 MHz (field strength of 11.8 T) with a 4.0 mm MAS probe in order to gain insight into the structural organization of the graphene oxide samples. ^{13}C chemical shifts are given relative to tetramethylsilane (TMS, $(^{13}CH_3)_4Si$), whose position is set to 0 ppm. The typical rotor spin rate was 11 kHz, and data was acquired following a spin-echo ($\pi/2 - \pi - \pi -$ *acquire*) pulse sequence (3000 scans). The delay between pulses, τ, was taken as the inverse spinning rate for rotosynchronization, and a 200s recycle delay was used to prevent signal saturation.

After phasing and background-correction the spectra were decomposed with Gaussian peaks using the software IGOR Pro.

2.15. X-ray photoelectron spectroscopy (XPS)

XPS spectra of GO were acquired using Thermo Scientific K-Alpha system with a monochromated Al Kα x-ray source ($h\nu$ = 1486.7 eV) and a hemispherical analyzer. The core-level spectra were acquired with a pass energy of 50.0 eV and a flood gun was used for charge compensation. The graphitic carbon peak was used as an internal reference. XPS peak fitting were performed by using *Avantage* software supplied along with the Thermo K-Alpha system. For the core-level spectra, a modified Shirley background is utilized for the background correction ("smart background"). The FWHM of the decomposed peaks are a function of the intrinsic photoelectron core-hole lifetimes, instrumental broadening, and film heterogeneity. The FWHM values for the various elements were allowed to float within a small range in the peak fitting routine. The functional group assignments of the C1s, O1s, S2p and N1s core-level were made based on literature assignments for well-understood systems.

2.16. Gaussian calculations

All geometry optimizations and frequency calculations were performed with the Gaussian 09 computational chemistry package using the M06 DFT functional and the 6-31 + G(d) basis set. Frequency calculations were subsequently performed on the optimized geometries to confirm that they were stationary states, and to obtain the thermal corrections to the free energy.

3. Results and discussion

3.1. Ozone evolution from GO?

UV–visible absorption spectroscopy suggested that ozone is present during the synthesis of GO using a modified Hummer's method [19], but it was not investigated whether ozone could evolve from thermal treatment of GO. Here, we investigated the decomposition of GO using a potentiometric ozone gas sensor (Fig. 1 a) and measured a linear voltage increase with the mass of GO, when using small enough amounts (<23 mg) properly spread out to avoid explosions in a GC-MS vial. Samples that exploded below 200 °C produced a non-reproducible higher signal response dependent on the level of aggregation and distribution of the sample in the reaction vessel. Given the possibilities of interfering substances in a metal-oxide based sensor, we could not definitively conclude that ozone was present. Therefore, temperature programmed desorption (TPD) gas analysis with mass spectrometric detection measurements with increasing temperature were conducted as a function of time and sample mass (Fig. 1 b). In a typical unexploded sample (14.4 mg) significant water loss was found between 52 °C and 140 °C as indicated by the detection of water, hydroxy and hydrogen radicals (H_2O, m/z = 18; $OH^{\bullet}$, m/z = 17; and $H^{\bullet}$, m/z = 1, in order of decreasing abundance) simultaneously peaking at 58 °C (4.5 min) with a shoulder peak at 87 °C (12.2 min). The major thermal event occurred at 186 °C (32.6 min) with the loss of CO_2 with a shoulder peak at 246 °C (44.8 min, CO_2, m/z = 44). The former peak is aligned with those of carbonyl, additional water loss, oxygen radical, hydroxyl radical, carbon, and hydrogen radical (CO, m/z = 28; H_2O, m/z = 18; $O^{\bullet}$, m/z = 16; $OH^{\bullet}$, m/z = 17; C, m/z = 12; $H^{\bullet}$ m/z = 1).

A peak at 225 °C (41.2 min, m/z = 48) compatible with the presence of ozone was detected, but the presence of sulfur monoxide (SO) provided a valid alternative explanation that could not be excluded. A simultaneous peak was measured with more than twice the relative intensity of that of the peak at 48 m/z, which was attributed to sulfur dioxide (SO_2 m/z = 64) [13]. These peaks are overlapped with shoulder peaks from water, carbon dioxide and hydroxyl radical (H_2O, m/z = 18; CO_2, m/z = 44; $OH^{\bullet}$, m/z = 17). In samples that explode, most peaks would appear simultaneously and at the same temperature with the exception of water and carbon dioxide (Fig. 1 c and Supplementary Fig. 2). We observed that the explosion tends to occur at lower temperature with bigger sample mass. However, comparison of unexploded and exploded samples of similar mass results in similar peak areas, even if they differed in intensity by one order of magnitude. Note that the thermal or photochemical decomposition from the suspected ozone to singlet oxygen on the carbon surface was not observed, unlike what has been previously reported for silica surfaces [33]. Monitoring for time-resolved singlet oxygen phosphorescence at 1270 nm upon the decomposition of GO at 200 °C indicates that singlet oxygen is not generated at the air/GO interface (data not shown). This is consistent with the absence of a molecular oxygen peak in our gas analysis via mass spectrometry.

In order to carry out higher accuracy formula identification for the peak at about 48 m/z we measured the mass spectra of GO in direct insertion experiments in comparison with ozone detection from an ozone generator. We analyzed the spectra using MassWorks software enhanced by the calibrated line-shape isotope profile search (CLIPS) analysis (Fig. 1 d and Supplementary Table 2). It can be seen that the mass error was below 1 mDa with a spectral accuracy of 99.49% in the case of generated ozone. In the case of GO we found the mass error to be about 3.3 mDa if we admit the formula to be SO, and ca. −14.5 mDa if we accept the formula to be O_3. The spectral accuracies in the latter two cases were quite similar, 96.69% and 96.24%, respectively. The comparison of the peak areas at m/z = 47.9697 and at m/z = 63.9591 in the spectrum of GO gives a ratio of 40.8%. This percentage is within instrumental variability error in the measurement of SO_2 gas. The NIST spectrum of SO_2 measured under electron ionization conditions shows that the peak of SO at m/z = 48 is about 49.3% of the peak of SO_2 at m/z = 64. These data indicate that the peak at m/z = 48 should very likely be assigned to SO rather than O_3. These results can be rationalized by hypothesizing the presence of peroxymonosulfate ester groups ($COOSO_3H$) on the surface of GO.

We still wonder if the high accuracy mass spectrometry results allow us to completely exclude that we did smell ozone after the

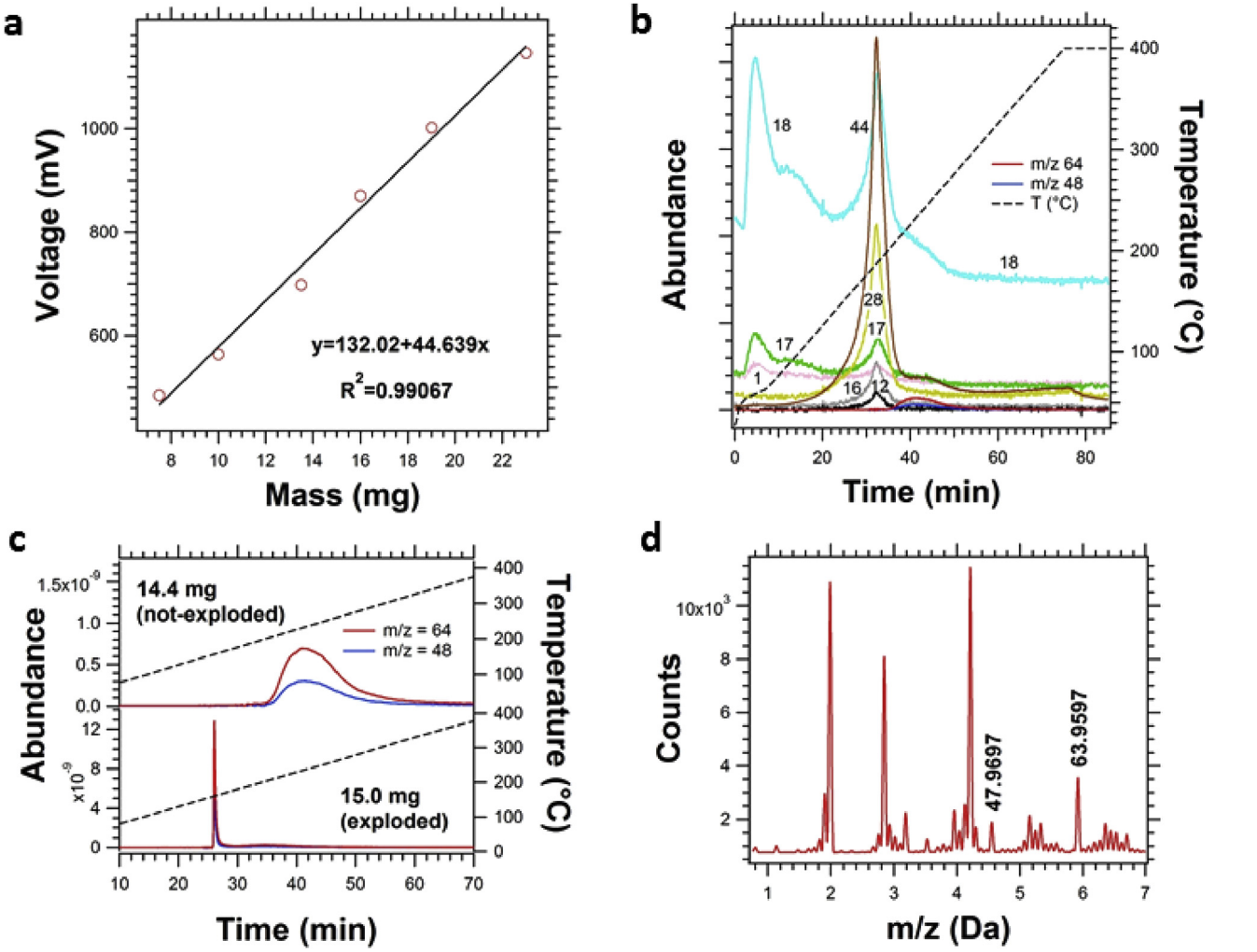

Fig. 1. (a), Potentiometric detection of ozone versus sample mass of unexploded GO. (b), Analysis of gases evolved from unexploded GO (14.4 mg) with time; *m*/*z* values are given along the traces or in legend for smaller peaks of interest; the temperature ramp (5 °C/min) is given as a dotted line. (c), Expanded profiles of the peaks at $m/z = 48$ and $m/z = 64$ traces of unexploded and exploded samples. (d), High accuracy mass spectrum resulting from MassWorks software analysis on a ~2 mg unexploded GO sample measured in a direct insertion experiment. (A colour version of this figure can be viewed online.)

thermally induced explosion mentioned above and did not detect ozone with our potentiometric sensor. It is quite possible that both our noses and the sensor detected SO instead of ozone. The detection of both SO and ozone are extremely challenging because their high reactivity makes detection of low amounts quite difficult. As shown below, in principle, the release of ozone from the thermal decomposition of GO is still a possibility.

3.2. Structure and morphology of GO

A structural model (Fig. 2 a) similar to the Lerf-Klinowski model was used as a working hypothesis in order to account for these observations. Our qualitative model includes lactols as previously proposed [34], carboxylic groups, anhydrides, ketones, mono- and di-substituted sulfate and peroxysulfate esters vicinal to epoxides, neighboring alcohols and epoxide groups [27], in addition to isolated sulfates esters and C—OH. Closed-ring peroxydisulfates resulting from a secondary reaction of peroxymonosulfates with a neighboring alcohol groups are also possible, even if in the following discussion we will mainly focus on peroxymonosulfates. The esters of Caro's acid (H_2SO_5) are relatively stable peroxides [35] similar to more common persulfates formed by reaction with $K_2S_2O_8$ [36,37]. Our mass spectrometry results indicate that the peroxymonosulfate esters decompose to SO_2 and H_2O.

The TEM image of our GO (Fig. 2 b) indicates the successful exfoliation of the precursor graphite with some degree of aggregation. The EDX spectra (data not shown) indicate that GO is very pure and contains only C, O, and S. The powdered X-ray diffraction of GO (Fig. 2 c) showed a peak at $2\theta = 9.95°$. An interlayer separation of 8.8 Å can be calculated from this result, a spatial distance greater than previously reported, suggesting a higher level of oxidation of GO. This is confirmed by the absence of a broad peak at approximately $2\theta = 18°$, showing that unreacted graphite is below the detection limit and the reaction proceeded to completion. The TEM image of the nanographite precursor is shown in Supplementary Fig. 3. The precursor material is comprised of 1–2 μm agglomerates or graphite nanocrystals of average size of 100 nm.

The knowledge that ozone is present under the Hummers' method synthetic conditions [18] prompted us to search for peroxides on the surface. Initially, the presence of peroxides was suggested by a standard colorimetric test (Supplementary Fig. 4). More accurately, we conducted a chemical titration of the peroxides, assuming them to be peroxymonosulfate ester groups ($COO-SO_3H$), using *N*,*N*-diethyl-p-phenyldiamine as a chromatic indicator followed by visible absorption spectroscopy (Supplementary Fig. 5).

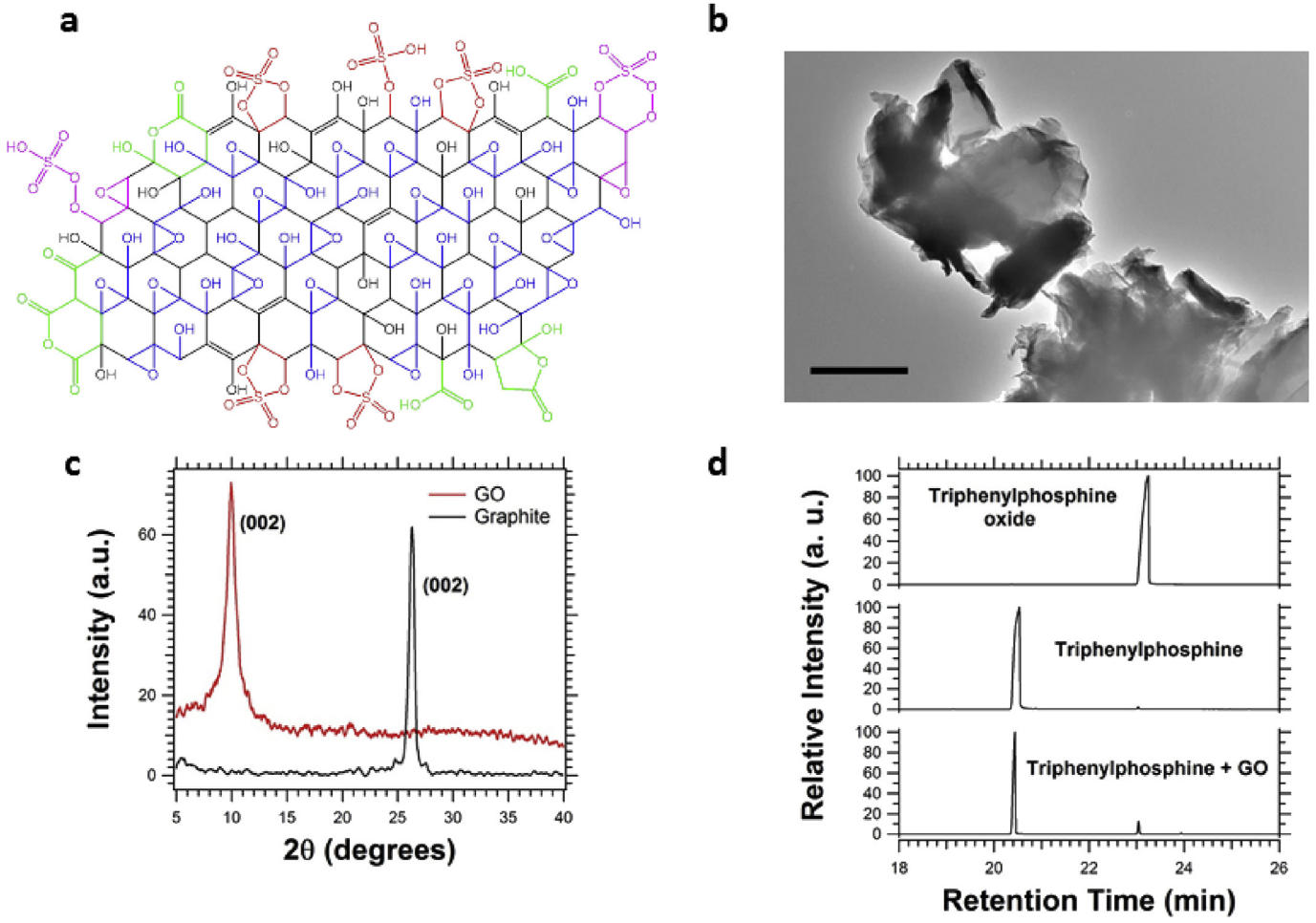

Fig. 2. (a) Structural model for GO emphasizing the presence of neighboring hydroxyl and epoxide groups (blue), isolated epoxide groups (brown), mono- and disubsituted sulfate esters (red), isolated hydroxylic groups (black), mono- and disubsituted peroxymonosulfate and peroxydisulfate esters with neighboring epoxides (purple), 5- and 6-membered ring lactols, ketone, anhydrides and carboxylic acids (green). (b), Transmission electron microscope image of GO; the scale bar is 1 μm. (c), X-ray diffraction spectra of GO and the precursor graphite. (d), Gas chromatogram of triphenylphosphine oxide, triphenylphosphine in acetonitrile, and the product of the reaction in acetonitrile between triphenylphosphine and GO; the conversion of triphenylphosphine to triphenylphosphine oxide revealed in this latter spectrum was 10% of the initial triphenylphosphine concentration. (A colour version of this figure can be viewed online.)

This method yielded a peroxymonosulfate ester amount of about 3.3% of total mass (g_{SO_5H}/g_{total}), 5.5% of the total oxygen ($g_O/g_{O_{total}}$), and 0.7% of total carbon ($g_C/g_{C_{total}}$). On the basis of the ICP-OES sulfur analysis (6.8%) we determine that peroxymonosulfate esters are 13.7% of sulfur containing groups, the rest being organic sulfates. The formation of peroxides was further confirmed by addition of triphenylphosphine to GO and formation of triphenylphosphine oxide was quantified by GC-MS measurements (Fig. 2 d). The amount of peroxides, assuming them to be peroxymonosulfate ester groups, was about 3.0% of total mass (g_{SO_5H}/g_{total}), 5.1% of the total oxygen ($g_O/g_{O_{total}}$), and 0.7% of total carbon ($g_C/g_{C_{total}}$). This assay indicates that peroxymonosulfate esters are 12.6% of sulfur containing groups. The percentage values determined by these chemical titrations are significant and may be underestimated, considering that *N*,*N*-diethyl-p-phenyldiamine and triphenylphosphine access to the surface peroxide groups is restricted.

3.3. Vibrational, NMR and XPS study of GO

In order to test our structural hypothesis we conducted a vibrational study of GO and chemically treated GO (Fig. 3 a and Supplementary Fig. 6) [26,38]. In our FT-IR analysis we compared the fingerprint region of anhydrous GO (1.6% water content) with that of GO treated with KI (KI-GO). The spectrum of KI-GO is for the most part very similar to that of GO with some notable changes. In previous work, prolonged treatment (1 week) of GO with KI has been used with the intention of reducing epoxide groups to phenols [24]. We found that a short KI treatment (1 h) mostly affects the stretching S=O or ν(S=O) of peroxymonosulfate esters at 1159 cm^{-1}, which confirms the assignment [36,37]. The approximate size of this band is shown as a Gaussian peak in the spectrum of GO. If this peak is subtracted from the spectrum of GO it yields a spectrum very similar to that of KI-GO. Corresponding to the peak at 1159 cm^{-1}, a O–O stretching of diminished intensity is found at 851 cm^{-1} in the spectrum of KI-GO, when compared to that of GO [17,39]. Peaks attributed to the symmetric and antisymmetric stretching sulfate esters bands are expected around 1070 cm^{-1} and between 1200 and 1280 cm-1, respectively, as in the case of sodium dodecyl sulfate [40]. The doublet at 1224 and 1266 cm^{-1}, was attributed to antisymmetric sulfate vibrations [13,40]. These bands are usually degenerate, but can become a doublet due to lower symmetry [40]. This splitting is compatible with the presence of mono- and di-substituted sulfate esters as shown in our structural model (Fig. 2 a). The corresponding symmetric sulfate band [40] is not visible because it is covered by the skeletal modes of C–C and C–O, ν(C–C) and ν(C–C) stretching measured at 1050 cm^{-1} [23,26].

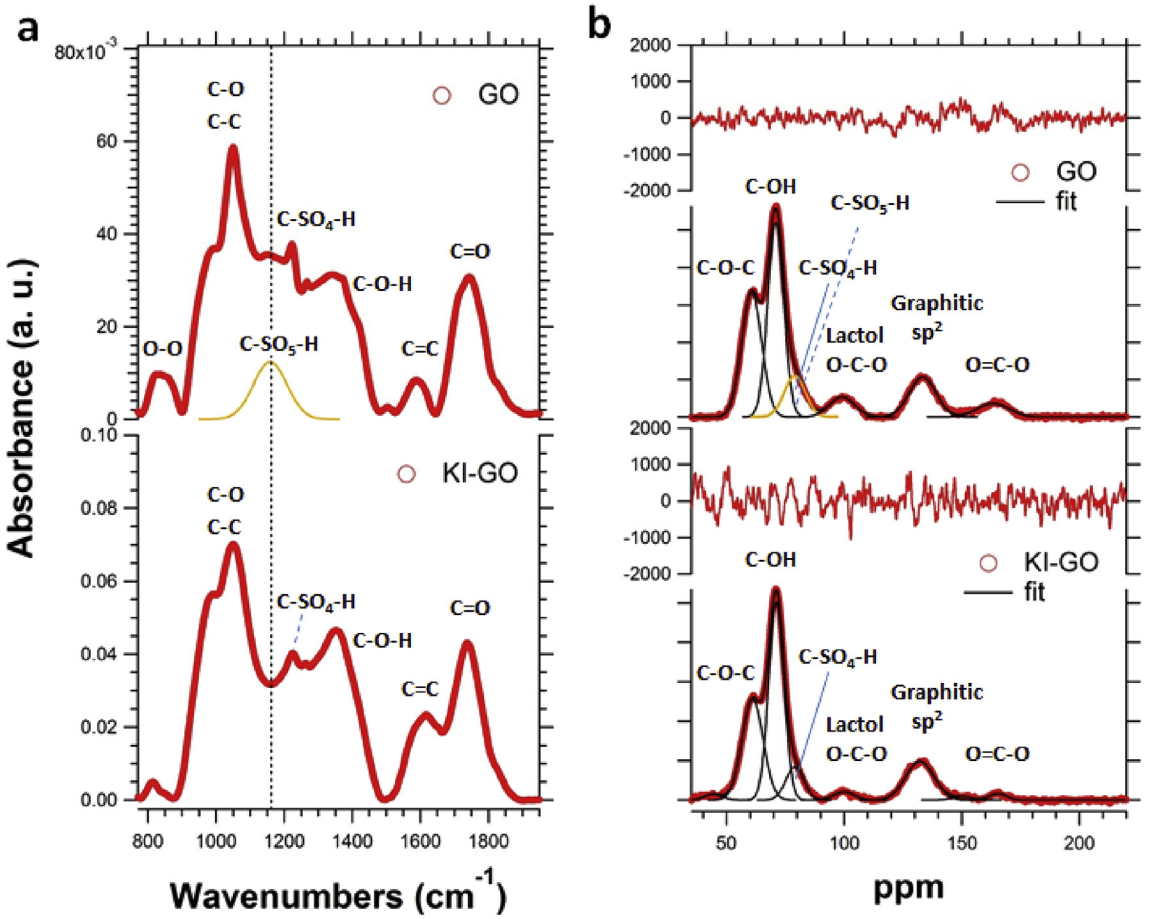

Fig. 3. (a) Gaussian decomposition of the medium infrared spectra of GO (top) and potassium iodide treated GO (KI-GO, bottom); the Gaussian peak attributed to peroxomonosulfate esters ($COOSO_3H$) is indicated in orange. (b), Gaussian decomposition of the $^{1}H-^{13}C$ cross-polarization NMR spectra of GO and KI-GO; the band dominated by peroxomonosulfate esters is also indicated in orange. Spectra were measured with 15 kHz MAS and a recycle delay of 2 s for 10,000 scans. (A colour version of this figure can be viewed online.)

No significant differences were detected in the highly crowded OH stretching region. The broad peak at 1370 cm^{-1} in GO was attributed to the bending COH or δ(COH) [23,26]. The same peak in KI-GO was measured at 1355 cm^{-1}. The C═C stretching at 1590 cm^{-1} was observed in GO [23,26] and it was found to increase and shift to 1615 cm^{-1} in KI-GO, which may be affected by a higher water content. This observation is explained by the reactivity of KI in favoring elimination of water from vicinal OH resulting from the reduction of peroxymonosulfate esters to monosulfate esters and alcohols by iodide. The broad peaks at 1745 cm^{-1} in GO and 1740 cm^{-1} in KI-GO are attributed to the carbonyl stretching or ν(C═O) [23,26], typical of carboxylic groups, ketones, anhydrides, and possibly lactols.

The NMR investigation of GO and KI-GO (Fig. 3 b, Supplementary Fig. 7, and Supplementary Table 3) provides further structural insights and supports the infrared assignments. We conducted Gaussian decomposition of the $^{1}H-^{13}C$ cross-polarization NMR spectra of GO and KI-GO, which should be regarded as a method for identifying distributions of Lorentzian sites of similar origin. A semi-quantitative comparison of the resulting peaks was carried out. Though this approach goes beyond what is conventionally accepted from cross-polarization spectra, which are thought to be unfit for extracting reliable quantitative information, we are convinced that comparison of the GO and KI-GO $^{1}H-^{13}C$ NMR spectra yield relative abundances of these functional groups. As shown in Fig. 3 a, the IR spectra reveal that only minimal structural changes exist between GO and KI-GO except for the persulfate groups and the C═C bonds, as confirmed by the similarity of the cross-polarization spectra themselves (Fig. 3 b), thus allowing a meaningful comparison of the $^{1}H-^{13}C$ NMR spectra in our case. Our Gaussian analysis of GO (KI-GO) revealed a main peak comprised of 29.6% (29.2%) of epoxide carbons at 61 ppm and 36.5% (41.3%) of alcohol carbon.

Shoulder bands of the main NMR feature accounting for 10.2% and 8.1% of carbon were detected at 79 ppm in GO and KI-GO, and the percentage difference (2.1% of total C or 21% between the two peaks) was explained by assuming the presence of peroxymonosulfate esters [41]. The decrease for KI-GO reflects the IR intensity decrease in the peak at 1159 cm^{-1}. Calculated spectra considering different neighboring functional groups were compatible with the peroxymonosulfate esters assignment (Supplementary Fig. 7). In the shoulder region at 79 ppm there other functional groups beside peroxymonosulfate esters, such as sulfates, OH or epoxy sites neighboring these groups and other minor groups [41].

The remaining part of the spectrum was in agreement with previous findings: 12.6% (15.1%) of total carbon consists of sp^2 carbon at 133 ppm (132 ppm), 6.0% (2.4%) is given by sp^3 carbon or lactols at 99 ppm (100 ppm), 5.1% (1.6%) is given by O═C−O carbon at 163 ppm (165 ppm). The observation of increased sp^2 carbon in KI-GO further confirms the occurrence of OH elimination following KI treatment. The MAS spin echo data (Supplementary Fig. 8,

Supplementary Table 4) exhibited a lower resolution, but confirmed the overall assignment and semi-quantitative analysis of the cross-polarization spectra. The percentage difference for the peaks at 79 ppm was 2.6% of total C or 27% between the two peaks. The MAS spin echo spectra and the $^{1}H-^{13}C$ NMR spectra allowed us to estimate that for every sixteen/seventeen alcohols groups there is approximately one peroxymonosulfate ester groups in GO.

XPS measurements of our GO were conducted for the core-level C1s, O1s, S2p, and N1s (Supplementary Fig. 9, and Supplementary Tables 5–9). The elemental analysis derived from the XPS spectra (see Supplementary Table 5) shows values which are significantly different from the bulk elemental analysis (see Supplementary Table 1) results. This often occurs given that XPS probes only the first few layers of the sample (<8 nm) due to the short mean-free-path of the emitted electrons, the samples may have atmospheric adsorbents on them resulting from air-transfer, and X-ray irradiation itself may initiate surface chemical changes. The spectral assignments of the C1s peaks have been made based on published literature. The occurrence of hydroperoxides (C–O–O–H) and persulfates (C–O–O–S) are consistent with the peaks observed at 286.2 eV and 289.0 eV, respectively [42], although they could also result from other carbon-containing functional groups. The emergence of a peak at 286.5 eV was observed in ozonized GO and attributed to C=O or C–O–C functional groups [16]. The emergence of peaks at 286 and 289 eV, was reported for ozonized graphene and assigned to C–O and C=O functional groups, respectively [43]. In both references [16] and [43], the presence of peroxides was not directly recognized. The C1s spectra of GO synthesized by oxidation of conventional graphite by means of water-enhanced ozone formation differ from our spectrum in terms of ratio of the main peaks and number of fitting peaks [19]. However, the peak at 286.6 eV attributed to C–O without mention of possible peroxides, does grow with higher ozone levels. Further evidence of the C–O–O–H and C–O–O–S peroxide groups is observed in the O1s spectrum at 533.6 eV and 534.7 eV, respectively [42]. The S2p spectrum exhibited the signature of different sulfur moieties. The biggest S2p3 peak could be assigned to mono- and di-substituted organic sulfates at 168.3 eV, given the proximity of the binding energy to that of known inorganic sulfates [44]. The peak at 169.8 eV was assigned to mono- and di-substituted organic persulfates. This assignment is justified given the high binding energy, above values previously reported for most sulfur-containing compounds, and the proximity to the binding energy of inorganic persulfates [45].

4. Mechanism of ozone evolution from GO

Postulated intermediates for the mechanism of the evolution of ozonized species were explored by DFT calculations at the M06/6-31-G(d) level, using small oxygenated 2D nanocarbon derivatives (Fig. 4). The formation of primary ozonide (POz, 1,2,3-trioxolane) proceeds by conventional ozonolysis of alkene bonds available on the sp^2-sp^3 carbon surface. POz is a resonance form of the Criegee intermediate (CI) which is hindered from conversion to a secondary ozonide (SOz) by the rigidity of the carbon network. Resonance stabilization of the POz and CI are possible by delocalization of a positive charge into the conjugated π-system by formation of a peroxidate or an open trioxide anion intermediate. The protonation of the latter can result in an open hydrotrioxide in a slightly non-spontaneous process ($\Delta G = 30.1$ kcal/mol).

The thermal decomposition of the POz resonance forms and the hydrotrioxide could lead to the release of ozone in slightly non-spontaneous and spontaneous steps with ΔG equal to 23.3 kcal/mol and −6.9 kcal/mol, respectively. Remarkably, the most favored reaction pathway involves the CI undergoing spontaneous protonation and rearrangement to a stable epoxy-hydroperoxide compound with a neighboring delocalized positive charge, lowering the Gibbs free energy by 78.1 kcal/mol. Alternatively, the CI can react with sulfuric acid to form a peroxymosulfate ester in a very spontaneous process ($\Delta G = -80.2$ kcal/mol) with a delocalized positive charge too. In both cases, the positive charges can be neutralized by electronic defects of the basal plane of GO.

The vicinal epoxide and hydroperoxide groups (or peroxymonosulfate groups) on the same ring can easily evolve to vicinal epoxide and alcohol groups via a homolytic cleavage of the O–O bond involving OH• and H• radicals. The epoxy-hydroperoxide and the epoxy-persulfate structures differ minimally in terms of stability ($\Delta G = -2.1$ kcal/mol), but both represent significantly deeper wells in the Gibbs free energy landscape. This observation alone may explain why ozone was not conclusively measured.

Considering the formation of GO proceeds in an excess of sulfuric acid, it is expected that most peroxides on the surface will be in the form of peroxymonosulfates rather than hydroperoxides. The energy values here reported have only a relative significance as they were obtained in the gas phase at 0 K, and our calculation did not take into consideration further possible reactions of ozone if it were to leave the carbon surface. We also did not conduct calculations on the possibility of a direct reaction of alcohols (C–OH) with Caro's acid (H_2SO_5), which is produced in the presence of sulfuric acid and hydrogen peroxide (H_2O_2). This reaction could also lead to peroxymonosulfate esters. Furthermore, the calculation we conducted on small 2D nanocarbon derivatives could be applicable to nanocarbons of different sizes and could be extended to explain the behavior of OD [28,29].

5. Conclusions

Overall, our results clearly indicate that ozonolysis plays a significant role in the formation of GO when using the Hummers' method and its modifications. The amount of ozone changes with water-content and temperature but is invariably present under commonly used reactions conditions [18,19]. Previous research led to the hypothesis that atomic oxygen and hydroxyl radical generated by reaction of ozone with manganese species, participate in the oxidation of graphite to yield GO [19]. Here we propose that the reaction equilibrium is driven to the formation of ozonide products by the ozone generated by the solution of sulfuric acid and permanganate and the available graphite precursor. Further protonation of the CI or reaction with sulfuric acid stabilizes the ozonides in the form of vicinal epoxides and hydroperoxides (or persulfates). It cannot be excluded that permanganate undergoes direct oxidative alkene addition [11], and atomic oxygen and hydroxyl radicals oxidize the carbon basal plane [19], but these alternative mechanisms would not explain the formation of vicinal epoxy-alcohol groups as satisfactorily as an ozonation mechanism.

We could not find definitive proof of ozone production upon heating the GO. An important aspect of the proposed mechanism is that it allows us to understand why the central region of partially oxidized graphite, in the course of conversion from the sulfuric acid/graphite intercalation compound, appears to be blue in optical micrographs obtained in reflection mode using a white incandescent light source [10]. This occurs before the edge-to-center attack of the oxidizing medium of sulfuric acid and permanganate has occurred. We infer that the blue color is due to trapped ozone penetrating the van der Waals layers of yet undisrupted graphite. Indeed, a small degree of oxidation is detected in the center region by Raman spectroscopy before visible chemical oxidation occurs [10]. Interestingly, similar blue images were observed with graphite intercalation compounds generated by using ammonium persulfate and sulfuric acid [14]. The reaction of persulfates and sulfuric acid

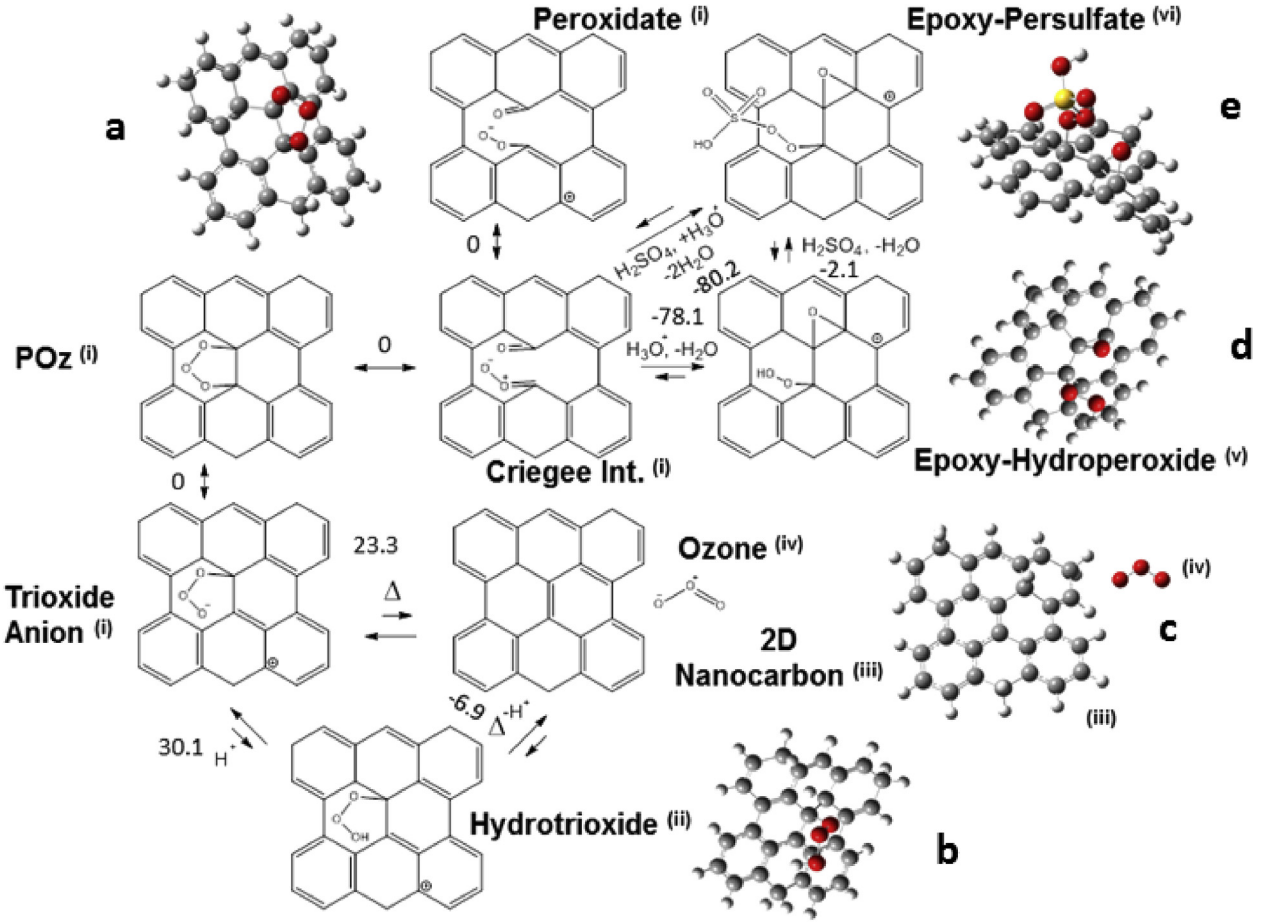

Fig. 4. Mechanism of ozone evolution with optimized geometries of peroxide intermediate on sp2-sp3 2D nanocarbon. (a), Structure of the POz on 2D nanocarbon, which is isoenergetic to the structures labelled with (i). (b), Structure of hydrotrioxide on 2D nanocarbon, which is isoenergetic to the structure labelled with (ii). (c), Structures of 2D nanocarbon and free ozone, corresponding to the structures labelled with (iii) and (iv). (d), Structure of epoxy-hydroperoxide compound, which is isoenergetic to the structures labelled with (v) and derived from the rearrangement of a protonated Criegee intermediate. (e) Structure of epoxy-persulfate, which is isoenergetic to the structure labelled with (vi). The numerical values of ΔG between two structures are indicated. The units are in kcal/mol (omitted for clarity). (A colour version of this figure can be viewed online.)

produces ozone too [46]. Therefore, we are led to wonder if other synthetic conditions used in the preparation of GO (e.g. the Brodie's method which requires $NaClO_3$ and HNO_3) may be associated with the presence of ozone in the initial phases of oxidation of graphite or at least other gases, but [23] no precedent was found in the literature.

It is likely that the initial oxidation by ozone allows hydrophilic sulfuric acid to get in molecular contact with hydrophobic graphite and promote its further exfoliation. Furthermore, the presence of multiple graphene layers in van der Waals interaction with each other may be necessary for ozone to be able to produce the initial oxidation of graphite to graphite ozonide layers, and pronounced curvature may not be required as in the case of SWNTs [21]. The presence of chemically trapped ozone suggests the possibility that sulfur-free ozonated graphene may be used as a precursor material for carrying out conventional ozonolysis as an alternative to direct ozonation under cryostatic conditions, provided ozone can be liberated efficiently. A catalyst may be needed to accomplish ozone release.

We identified and quantified the peroxymonosulfate esters remaining on the surface before and after KI treatment by NMR. Our analysis indicates about one peroxymonosulfate ester or one peroxydisulfate ester for every sixteen/seventeen alcohol groups. This estimate is consistent with the percentages of carbon belonging to peroxymonosulfate esters with respect to the total carbon functional groups determined by chemical methods (0.7% $g_C/g_{C_{total}}$) and the elemental analysis. The colorimetric detection of surface-bound peroxymonosulfate esters and trapping of oxygen with triphenylphosphine both indicate that the GO prepared by Hummers' method is much more reactive than previously appreciated. For example this likely explains the observation that many proteins on GO are deactivated not just by nonspecific interactions [6] but by direct oxidation involving persulfates [47]. The oxidative damage can be prevented by converting the persulfate esters to alcohols or other less reactive functional groups via mild heating or chemical treatment. Also, the observed antibacterial and cytotoxic properties of GO [7] can be attributed to surface peroxides. These findings do not exclude that OD may also play a role [8].

Intramolecular H-bonding of these peroxysulfate groups may explain the enhanced proton-conductivity in ozonated GO [48]. The high levels of peroxymonosulfate esters measured in our GO (42% oxygen content), are not necessarily unique to the specific synthetic conditions we have used. The generality of this conclusion is supported by comparison of the data presented here with IR and NMR evidence related to a variety of Hummers' method conditions previously reported [11]. However, the generalization of the proposed mechanism and peroxide functional groups requires the analytical protocol described herein to GO synthesized under systematic modifications of the Hummer's method. The investigation of directly ozonated graphite [17], GO [16], and graphene [43] will

allow explorations of the functional groups produced by ozonolysis without the interference of other groups. The size of the graphite precursor is expected to play a role the in determining the reactivity toward ozonation, indeed, our nanographite is more reactive than micrometric-size graphite, and may be more prone to ozonation. These investigations are beyond the scope of the present study.

Our findings indicate that our modified Lerf-Klinowsky model is a better structural model than the Szabo-Dékány model and accounts for a sterically hindered ozonolysis on progressively oxidized graphite. The main reason for this is that the Lerf-Klinowsky structure remains intrinsically more rigid than the Szabo-Dékány structure. The latter structure should be even more prone to deep oxidation than the former and even more peroxides would be expected. The presence of acid persulfate, sulfate esters, and some hydroperoxides can provide an alternative explanation for the unusual acidity of GO (pH = 2–3). The high-energy barriers among these species calculated in the gas phase is likely to be significantly lower in solution. These observations and improved structural model will open up new vistas in the chemistry and the applications of GO, and the design of better-performing GO-based materials.

Acknowledgments

The authors wish to thank Ihor Kopka for preliminary data and his initial hypothesis about the role of ozone in GO. The authors thank Peter Ratsep of Shimadzu Scientific Instruments and Yongdong Wang of Cerno Bioscience for the high accuracy mass spectrometry analysis. The authors thank Jacopo Samson (Hunter College) for assistance with the TEM measurements, Colleen Brent (Hunter College) for help with the ozone potentiometric measurements, Malathi Kalyanikar and Eric Garfunkel at Rutgers University for the XPS measurements. Also, the authors thank Albert Tamashausky of Asbury Carbons for providing access to proprietary nanographite products and technical assistance. S.G., M.V., C.M.D., L.C.F. wish to acknowledge National Science Foundation Integrative Graduate Education and Research Traineeship Grant (NSF, IGERT 0965983 at Hunter College), and CHE-1610755 (C.M.D.). M.V. wishes to acknowledge Vito Di Noto for useful discussion, AFOSR grant FA9550-16-1-0279, and Medgar Evers College for internal funding. Hunter College infrastructure is supported by CUNY, NSF, NIH, including RCMI National Institute on Minority Health and Health Disparities (8G12 MD007599). E.J. B. would like to thank the Dormitory Authority of the State of New York (DASNY) through the Graduate Research and Technology Initiative (GRTI) for funding for the Hiden HPR-20 system. A.G. thanks the National Science Foundation (CHE1464975) and PSC-CUNY (68125-0046) for funding. The NMR data collected at NYSBC, of which CUNY faculty are members, was made possible by a grant from NYSTAR. This research utilized the resources of the National Energy Research Center (NERSC), which is supported by the Office of Science of the Department of Energy under Contract No. DE-AC02-05CH11231.

Appendix A. Supplementary data

Supplementary data related to this article can be found at http://dx.doi.org/10.1016/j.carbon.2017.06.092.

References

[1] Y. Si, E.T. Samulski, Synthesis of water soluble graphene, Nano Lett. 8 (2008) 1679–1682.
[2] D.R. Dreyer, S. Park, C.W. Bielawski, R.S. Ruoff, The chemistry of graphene oxide, Chem. Soc. Rev. 39 (2010) 228–240.
[3] S.-S. Li, K.-H. Tu, C.-C. Lin, C.-W. Chen, M. Chhowalla, Solution-processable graphene oxide as an efficient hole transport layer in polymer solar cells, ACS Nano 4 (2010) 3169–3174.
[4] Y. Li, Q. Wu, Y. Zhao, Y. Bai, P. Chen, T. Xia, D. Wang, Response of MicroRNAs to in vitro treatment with graphene oxide, ACS Nano 8 (2014) 2100–2110.
[5] M. Sopotnik, A. Leonardi, I. Krizaj, P. Dusak, D. Makovec, T. Mesaric, N. Poklar Ulrih, I. Junkar, K. Sepcic, D. Drobne, Comparative study of serum protein binding to three different carbon-based nanomaterials, Carbon 95 (2015) 560–572.
[6] X. Sun, Z. Feng, T. Hou, Y. Li, Mechanism of graphene oxide as an enzyme inhibitor from molecular dynamics simulations, ACS Appl. Mater. Interfaces 6 (2014) 7153–7163.
[7] L. Hui, J.-G. Piao, J. Auletta, K. Hu, Y. Zhu, T. Meyer, H. Liu, L. Yang, Availability of the basal planes of graphene oxide determines whether it is antibacterial, ACS Appl. Mater. Interfaces 6 (2014) 13183–13190.
[8] A. Pattammattel, C.L. Williamsa, P. Pandea, W.G. Tsuia, A.K. Basua, C.V. Kumara, Biological relevance of oxidative debris present in as-prepared graphene oxide, RSC Adv. 5 (2015) 59364–59372.
[9] W.S. Hummers, R.E. Offeman, Preparation of graphitic oxide, J. Am. Chem. Soc. 80 (1958) 1339.
[10] A.M. Dimiev, J.M. Tour, Mechanism of graphene oxide formation, ACS Nano 8 (2014) 3060–3068.
[11] J.H. Kang, T. Kim, J. Choi, J. Park, Y.S. Kim, M.S. Chang, H. Jung, K.T. Park, S.J. Yang, C.R. Park, Hidden second oxidation step of Hummers method, Chem. Mater. 28 (2015) 756–764.
[12] A. Dimiev, D.V. Kosynkin, L.B. Alemany, P. Chaguine, J.M. Tour, Pristine graphite oxide, J. Am. Chem. Soc. 134 (2012) 2815–2822.
[13] S. Eigler, C. Dotzer, F. Hof, W. Bauer, A. Hirsch, Sulfur species in graphene oxide, Chem. Eur. J. 19 (2013) 9490–9496.
[14] A.M. Dimiev, S.M. Bachilo, R. Saito, J.M. Tour, Reversible formation of ammonium persulfate/sulfuric acid graphite intercalation compounds and their peculiar raman spectra, ACS Nano 6 (2012) 7842–7849.
[15] Y. Mulyana, M. Uenuma, Y. Ishikawa, Yukiharu Uraoka, Reversible oxidation of graphene through ultraviolet/ozone treatment and its nonthermal reduction through ultraviolet irradiation, J. Phys. Chem. C 118 (2014) 27372–27381.
[16] F. Yang, M. Zhao, Z. Wang, H. Ji, B. Zheng, D. Xiao, L. Wu, Y. Guo, The role of ozone in the ozonation process of graphene oxide: oxidation or decomposition? R. Soc. Chem. Adv. 4 (2014) 58325–58328.
[17] S.D. Razumovskii, V.N. Gorshenev, A.L. Kovarskii, A.M. Kuznetsov, A.N. Shchegolikhin, Carbon nanostructure reactivity: reactions of graphite powders with ozone, Fullerenes, Nanotub. Carbon Nanostructures 15 (2007) 53–63.
[18] T.S. Dzhabiev, N.N. Denisev, D.N. Moiseev, A.E. Shilov, formation of ozone during the reduction of potassium permanganate in sulfuric acid solutions, Chem. Kinet. Catal. 79 (2004) 1755–1760.
[19] J. Chen, Y. Zhang, M. Zhang, B. Yao, Y. Li, L. Huang, C. Li, G. Shi, Water-enhanced oxidation of graphite to graphene oxide with controlled species of oxygenated groups, Chem. Sci. 7 (2016) 1874–1881.
[20] R.C. Chapleski Jr., J.R. Morris, D. Troya, A theoretical study of the ozonolysis of C60: primary ozonide formation, dissociation, and multiple ozone additions, Phys. Chem. Chem. Phys. 16 (2014) 5977–5986.
[21] Á. Castillo, L. Lee, A. Greer, Encapsulation and convex-face thiozonolysis of triatomic sulfur (S_3) with carbon nanotubes, J. Phys. Org. Chem. 25 (2012) 42–49.
[22] S.N. Chu, S. Sands, M.R. Tomasik, P.S. Lee, V.F. McNeill, Ozone oxidation of surface-adsorbed polycyclic aromatic hydrocarbons: role of PAH-surface interaction, J. Am. Chem. Soc. 132 (2010) 15968–15975.
[23] T. Szabo, O. Berkesi, P. Forgo, K. Josepovits, Y. Sanakis, D. Petridis, I. Dekany, Evolution of surface functional groups in a series of progressively oxidized graphite oxides, Chem. Mater. 18 (2006) 2740–2749.
[24] H. He, J. Klinowski, M. Forster, A. Lerf, A new structural model for graphite oxide, Chem. Phys. Lett. 287 (1998) 53–56.
[25] M. Acik, G. Lee, C. Mattevi, A. Pirkle, R.M. Wallace, M. Chhowalla, K. Cho, Y. Chabal, The role of oxygen during thermal reduction of graphene oxide studied by infrared absorption spectroscopy, J. Phys. Chem. 115 (2011) 19761–19781.
[26] T. Szabo, O. Berkesi, I. Dekany, DRIFT study of deuterium-exchanged graphite oxide, Carbon 43 (2005) 3181–3194.
[27] W. Cai, R.D. Piner, F.J. Stadermann, S. Park, M.A. Shaibat, Y. Ishii, D. Yang, A. Velamakanni, S.J. An, M. Stoller, J. An, D. Chen, R.S. Ruoff, Synthesis and solid-state NMR structural characterization of ^{13}C-labeled graphite Oxide, Science 321 (2008) 1815–1817.
[28] A. Bonanni, A. Ambrosi, C.K. Chua, M. Pumera, Oxidation debris in graphene oxide is responsible for its inherent electroactivity, ACS Nano 8 (2014) 4197–4204.
[29] X. Chen, B. Chen, Direct observation, molecular structure, and location of oxidation debris on graphene oxide nanosheets, Environ. Sci. Technol. 50 (2016) 8568–8577.
[30] G. Metz, X.L. Wu, S.O. Smith, Ramped-amplitude cross polarization in magic-angle-spinning NMR, J. Magn. Reson. Ser. A 110 (1994) 219–227.
[31] A.E. Bennett, C.M. Rienstra, M. Auger, K.V. Lakshmi, R.G. Griffin, Heteronuclear decoupling in rotating solids, J. Chem. Phys. 103 (1995) 6951–6958.
[32] C.R. Morcombe, K.W. Zilm, Chemical shift referencing in MAS solid state NMR, J. Magn. Reson. Ser. A 162 (2003) 479–486.
[33] D. Bartusik, D. Aebisher, G. Ghosh, M. Minnis, A. Greer, Fluorine end-capped optical fibers for photosensitizer release and singlet oxygen production, J. Org. Chem. 77 (2012) 4557–4565.

[34] W. Gao, L.B. Alemany, L. Ci, P.M. Ajayan, New insights into the structure and reduction of graphite oxide, Nat. Chem. 1 (2009) 403–408.
[35] H. Hussain, I.R. Green, I. Ahmed, Journey describing applications of oxone in synthetic chemistry, Chem. Rev. 113 (2013) 3329–3371.
[36] E.H. Appelman, L.J. Basile, H. Kim, J.R. Ferraro, Molecular vibrational spectra of potassium peroxymonosulfate, $KHS0_5$ and $KHS0_5$ - H_20, and of the aqueous peroxymonosulfate ion, Spectrochim. Acta 41A (1985) 1295–1300.
[37] A.I. Lapshin, K.A. Tleulieva, High-temperature ir-spectroscopic investigation of the structural and kinetic characteristics of sulfate formation by thermal decomposition of potassium persulfate, J. Appl. Spectrosc. 24 (1976) 484–487.
[38] M. Acik, G. Lee, C. Mattevi, M. Chhowalla, K. Cho, Y.J. Chabal, Unusual infrared-absorption mechanism in thermally reduced graphene oxide, Nat. Mater. 9 (2010) 840–845.
[39] J. Liu, C. Chen, C. He, J. Zhao, X. Yang, H. Wang, Synthesis of graphene peroxide and its application in fabricating super extensible and highly resilient nano-composite hydrogels, ACS Nano 6 (2012) 8194–8202.
[40] T. Kawai, J. Umemura, T. Takenaka, Fourier Transform Infrared Study on the Phase Transitions of a Sodium Dodecyl Sulfate-water System, vol. 61, Bulletin of the Institute of Chemical Research, Kyoto University, 1983, pp. 314–323.
[41] A. Lerf, H. Heb, T. Riedl, M. Forster, J. Klinowski, ^{13}C and ^{1}H MAS NMR studies of graphite oxide and its chemically modified derivatives, Solid State Ionics 101–103 (1997) 857–862.
[42] A. Dilks, The identification of peroxy-features at polymer surfaces by ESCA, J. Polym. Sci. Part A. Polym. Chem. 19 (1981) 1319–1327.
[43] J. Yuan, L.-P. Ma, S. Pei, J. Du, Y. Su, W. Ren, H.-M. Cheng, Tuning the electrical and optical properties of graphene by ozone treatment for patterning monolithic transparent electrodes, ACS Nano 7 (2013) 4233–4241.
[44] G. Beamson, D. Briggs, High Resolution XPS of Organic Polymers, the Scienta ESCA300 Database, Wiley, Chichester, 1992.
[45] X.-R. Yu, F. Liu, Z.-Y. Wang, Y. Chen, Auger parameters for sulfur-containing compounds using a mixed aluminum-silver excitation source, J. Electron Spectrosc. Relat. Phenom. 50 (1990) 159–166.
[46] E.K. Rideal, Ozone, Constable & Company LTD, London, 1920, p. 31.
[47] A.R. Chesney, C.J. Booth, C.B. Lietz, L. Li, J.A. Pedersen, Peroxymonosulfate rapidly inactivates the disease-associated prion protein, Environ. Sci. Technol. 50 (2016) 7095–7105.
[48] W. Gao, G. Wu, M.T. Janicke, D.A. Cullen, R. Mukundan, J.K. Baldwin, E.L. Brosha, C. Galande, P.M. Ajayan, K.L. More, A.M. Dattelbaum, P. Zelenay, Ozonated graphene oxide film as a proton-exchange membrane, Angew. Chem. Int. Ed. 53 (2014) 3588–3593.

Further reading

[49] C. Mattevi, G. Eda, S. Agnoli, S. Miller, K.A. Mkhoyan, O. Celik, D. Mastrogiovanni, G. Granozzi, E. Garfunkel, M. Chhowalla, Evolution of electrical, chemical, and structural properties of transparent and conducting chemically derived graphene thin films, Adv. Funct. Mater. 19 (2009) 2577–2583.
[50] M. Patel, W. Feng, K. Savaram, M.R. Khoshi, R. Huang, J. Sun, E. Rabie, C. Flach, R. Mendelsohn, E. Garfunkel, H. He, Microwave enabled one-pot, one-step fabrication and nitrogen doping of holey graphene oxide for catalytic applications, Small 11 (2015) 3358–3368.
[51] U. Gelius, P.F. Hedén, J. Hedman, B.J. Lindberg, R. Manne, R. Nordberg, C. Nordling, K. Siegbahn, Molecular spectroscopy by means of ESCA iii. Carbon compounds, Phys. Scr. 2 (1970) 70–80.
[52] G.P. López, D.G. Castner, B.D. Ratner, XPS O 1s binding energies for polymers containing hydroxyl, ether, ketone and ester groups, Surf. Interface Anal. 17 (1991) 267–272.
[53] G. Barth, R. Linder, C. Bryson, Advances in charge neutralization for XPS measurements of nonconducting materials, Surf. Interface Anal. 11 (1988) 307–311.
[54] J.S. Brinen, S. Greenhouse, P.K. Jarrett, XPS and SIMS studies of biodegradable suture materials, Surf. Interface Anal. 17 (1991) 259–266.
[55] F. Bournel, C. Laffon, P. Parent, G. Tourillon, Adsorption of some substituted ethylene molecules on Pt(111) at 95 K Part 1: NEXAFS, XPS UPS Stud. Surf. Sci. 350 (1996) 60–78.
[56] G. Beamson, D.T. Clark, N.W. Hayes, D.S.-L. Law, Effect of crystallinity of the XPS spectrum of poly(ethylene terephtalate), Surf. Sci. Spectra 3 (1994) 357–365.